810575

Wind-Tunnel Measurements of Wing-Canard Interference and a Comparison with Various Theories

T. W. Feistel, V. R. Corsiglia, and D. B. Levin*
*NRC Associate
Large Scale Aerodynamics Branch
Ames Research Center, NASA
Moffett Field, California

Wind-tunnel tests and analyses of the aerodynamics of wing-canard combinations for low-speed applications are described. The experimental data show that the interference between the wing and canard was favorable to the $C_{L_{max}}$ of the canard and did not degrade the $C_{L_{max}}$ of the wing, provided the canard was properly located vertically with respect to the wing. Comparison of these measurements with calculated results from a vortex-lattice panel code and with the classical Prandtl-Munk theory indicated that the panel code gave excellent results for lift and induced drag at moderate C_L. The Prandtl-Munk theory gave conservative results for induced drag. It was found, on the basis of a simple analysis using the Prandtl-Munk theory, that the L/D of a typical commuter transport that was canard-configured could be higher than the L/D of a transport with the tail aft, if the canard aspect ratio was greater than the wing aspect ratio.

ABSTRACT

CANARD-CONFIGURED AIRCRAFT DESIGNS have played a historic role in aeronautical research. However, only in the past decade or two has a canard been incorporated into a significant number of aircraft designs. Powered flight began with the Wright Flyer, which was a canard-configured aircraft. Unfortunately, however, that aircraft was longitudinally unstable and the misconception arose that all canard aircraft would be unstable in pitch, irrespective of the placement of the center of gravity. In the early years of aircraft development, the canard concept was dropped in favor of conventional tail-aft designs. It was not until the 1960s that canards were again seriously considered for several high-speed designs. For example, in the United States' supersonic transport program, a canard was initially considered; because of several problems with aerodynamic interference, however, the idea was abandoned. For example, the canard wake passed around the vertical stabilizer and resulted in erratic directional behavior. Canard tip vortices

0096-736X/82/9002-2026$02.50

interfered with the engine inlets, and pitching-moment control reversal occurred in some cases because of interference between the canard wake and the low-aspect-ratio wing. In spite of these difficulties, a retractable canard was incorporated into the Soviet SST. In the same time period during which the SSTs were being developed, the Saab Viggen fighter aircraft successfully achieved a favorable interference between a close-coupled canard and a low-aspect-ratio wing; as a result, vortex bursting was delayed and an increased C_L was achieved. In recent years, many of the prospective designs for new high-speed fighter aircraft have incorporated canards to achieve very high maneuvering capability.

Canards have not, however, been widely applied to either transport or light aircraft. The most notable expection is the general aviation designs by Burt Rutan (1)*. Those aircraft, which have generated considerable interest in the application of canards, have clearly demonstrated that when the center of gravity is properly located, a canard-configured aircraft is longitudinally stable and can have very desirable stall characteristics. Another and neglected application for canards is in high-lift STOL aircraft. Existing STOL designs are limited by large trim penalties in lift and drag. If a canard configuration were used on these aircraft, the sizeable lift advantage derived from all surfaces lifting up, together with the possibility of favorable interference between the canard and wing, could result in higher trimmed lift together with a lower overall level of sophistication for the high-lift devices compared with those of a tail-aft design.

In recent years, several studies have been published that dealt with the comparison of the drag characteristics between canard- and tail-configured aircraft (2-4). The published studies have relied on the Prandtl-Munk theory (5) to predict the induced drag. Wolkovitch (4) considered canards and wings of equal spans and concluded that there was an induced drag advantage over tail configurations. Shorter canard spans were studied by McLaughlin (2) who concluded that the induced drags of his canard configurations were generally higher than those of comparable tail-aft configurations. These two studies are in agreement, and they demonstrate that the induced drag is strongly dependent on the canard span.

The present paper reports on a research effort at Ames Research Center into canard configurations for low-speed applications. Systematic tests have been conducted in Ames' 7- by 10-Foot Wind Tunnel to explore various combinations of wing-canard vertical and horizontal positioning. There were three purposes for these tests: (1) to investigate potential improved stalling characteristics over conventional tail-aft configurations, (2) to investigate the existence of a $C_{L_{max}}$ advantage, and (3) to determine induced drag levels. Individual force and moment measurements were made on the wing and canard, both alone and in combination. These measurements are compared in this paper with calculations made using the Prandtl-Munk theory, and with a vortex-lattice panel code. The application that is considered here, in interpreting the results of this study, is a light transport aircraft used for short-haul operations. Such an aircraft would have a high-aspect-ratio straight wing instead of the low-aspect-ratio swept wings of the fighter and SST applications studied in the past.

NOMENCLATURE

AR	aspect ratio
b	span
c	chord
C_D	drag coefficient
C_{D_o}	minimum drag coefficient
C_L	lift coefficient = $L/q\ S_W$
C_M	pitching moment coefficient
C_{M_o}	C_M at zero lift

*Numbers in parentheses designate References at end of paper.

g	gap, vertical distance between surfaces
$\bar{g} \equiv \frac{g}{c_w}$	dimensionless gap
ℓ	stagger, horizontal distance between surfaces
$\bar{\ell} \equiv \frac{\ell}{c_w}$	dimensionless stagger
L/D	lift-to-drag ratio
q	dynamic pressure
S	surface area
α	angle of attack
σ	coefficient of Prandtl-Munk interference term

Subscripts

c	canard
i	induced
t	tail
w	wing

MODEL DESCRIPTION AND TEST DETAILS - A two-view sketch of the model that was tested in the 7- by 10-Foot Wind Tunnel at Ames Research Center is shown in Fig. 1. The model was designed so that the surfaces could be arranged in various positions with respect to one another, and so that the forces could be measured on each surface individually. To accomplish this, the forward surface was supported by a separate internal balance, and the force on the entire model was measured on the wind-tunnel balance system. The vertical spacing (gap) was changed by moving the aft surface vertically, and the axial spacing (stagger) was changed by use of a spacer in the body. Two lengths of the body were tested. The forward surface (canard) had an area one-half that of the aft surface (wing) and was always set at 2° incidence with respect to the wing. The wing and canard were unswept and had no twist, taper, or dihedral. The airfoil section of both was GA(W)-2, and the aspect

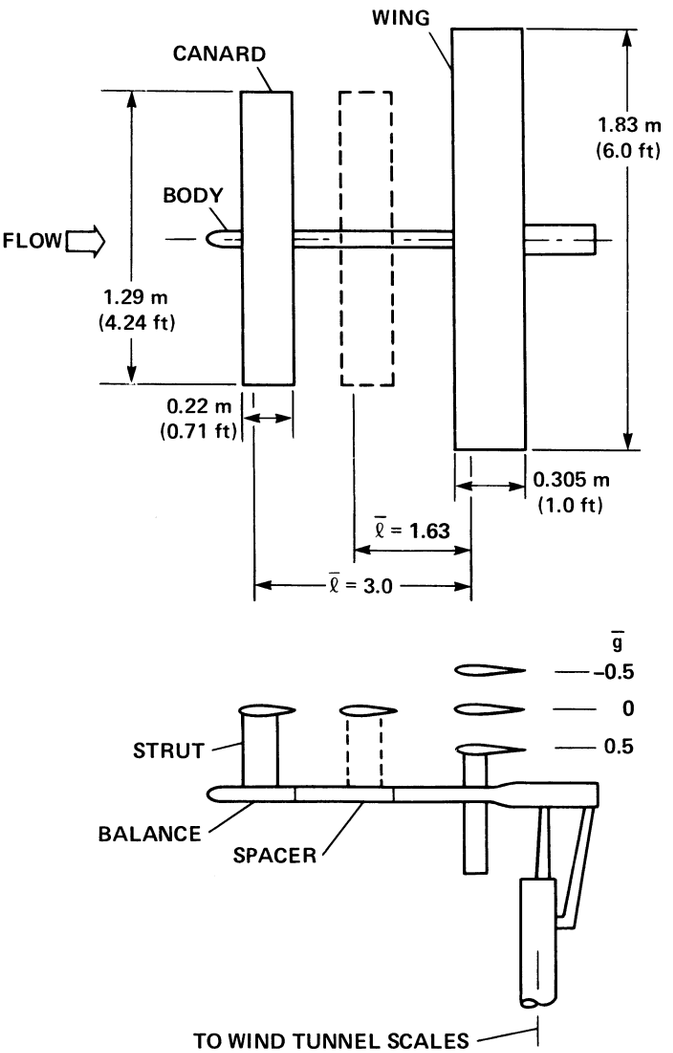

Fig. 1 - Two-view sketch of wing-canard interference model

ratio of both was 6. Table 1 gives additional details of the model and on the test conditions. The various combinations of gap and stagger that were tested are also listed in Table 1. Figure 2 shows the installation for both the short and long bodies.

Reynolds number based on wing chord was 1.4×10^6. Angle of attack was usually varied from $\alpha = -2°$ to $\alpha = 22°$, which is past the stall angle of attack. No wind-tunnel wall corrections were applied to the data (unless noted). However, the data were corrected for the support system tares by testing with the wing and canard removed. This tare effect (of the body and its support and of the wing and canard

Table 1 - Wing and Canard Geometry, Test Conditions, and Spacing

Characteristic	Geometry	
	Wing	Canard
Aspect ratio	6	6
Area, m^2 (ft^2)	0.56 (6)	0.28 (3)
Span, m^2(ft)	1.83 (6)	1.29 (4.24)
Chord, m (ft)	0.3 (1)	0.22 (0.71)
Planform	Rectangular	Rectangular
Taper, twist, dihedral	0	0
Section	GA(W-2)	GA(W)-2
Test conditions		
Angle-of-attack range	-2° to 22°	
Wind-tunnel dynamic pressure, kN/m^2 (lb/ft^2)	2.9 (60)	
Canard incidence relative to wing incidence	2°	
Wing and canard spacings tested, wing chords		
Vertical (gap)	Horizontal (stagger)	
+1/2 (high canard)	1.63 (short coupled)	
-1/2 (low canard)	1.63	
0	1.63	
-1/2	3.0 (long coupled)	
+1/2	3.0	

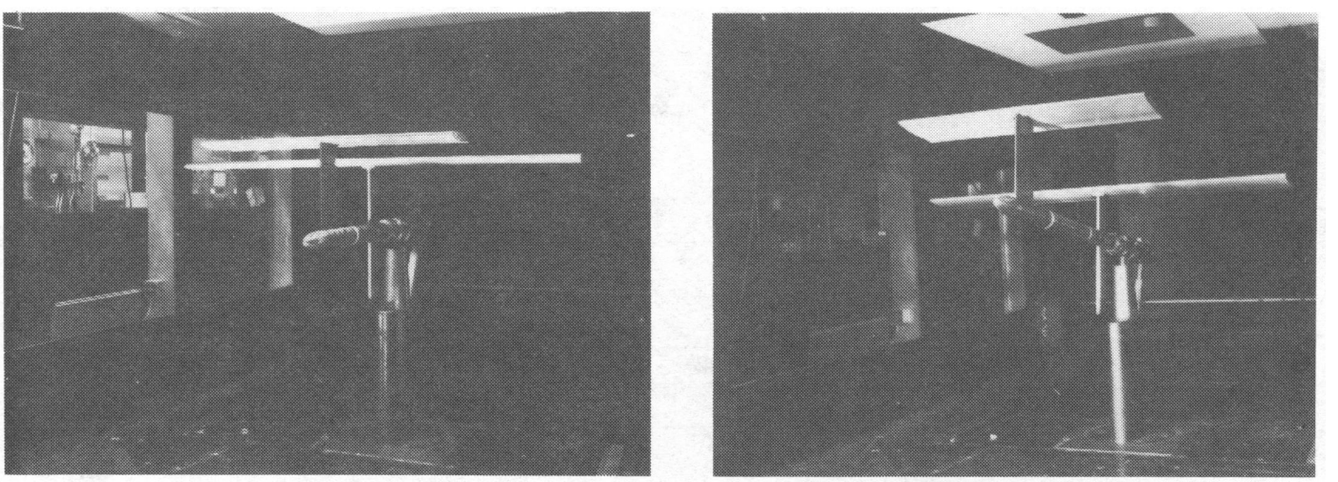

(a) Short body, $\bar{\ell}_C$ = 1.63 (b) Long body, $\bar{\ell}_C$ = 3.0

Fig. 2 - Wing-canard Model in 7- by 10-Foot Wind Tunnel

struts) was subtracted from the uncorrected measurements for all the data reported here. No roughness was applied to the model.

The aerodynamic coefficients for the wing and canard individually and combined are based on the wing area. The moment-center for pitching moment was located vertically at the level of the wing and horizontally at the centroid of the wing and canard areas; thus, it was one-third the distance from the wing quarter chord to the canard quarter chord.

DATA ANALYSIS

Figure 3 presents typical data for a wing-canard combination. For these data, the wing was mounted 0.5 wing chord below the level of the canard (canard high), and the distance between the wing and the canard quarter chords was 1.63 wing chords (i.e., $\bar{g} = +0.5$, $\bar{\ell} = 1.63$). The lift curves show the canard lift, the wing lift, and the combined lift separately. The wing lift is derived by subtracting the canard lift from the combined lift. As can be seen, the canard stalls at a much lower angle of attack than the wing, but maintains a high level of lift after stall. The $C_{L_{max}}$ of the configuration can be increased by increasing the $C_{L_{max}}$ of the canard. However, in order to have the pitching moment break stable at stall (as it does in Fig. 3) the canard should still stall at a slightly lower angle of attack than the wing.

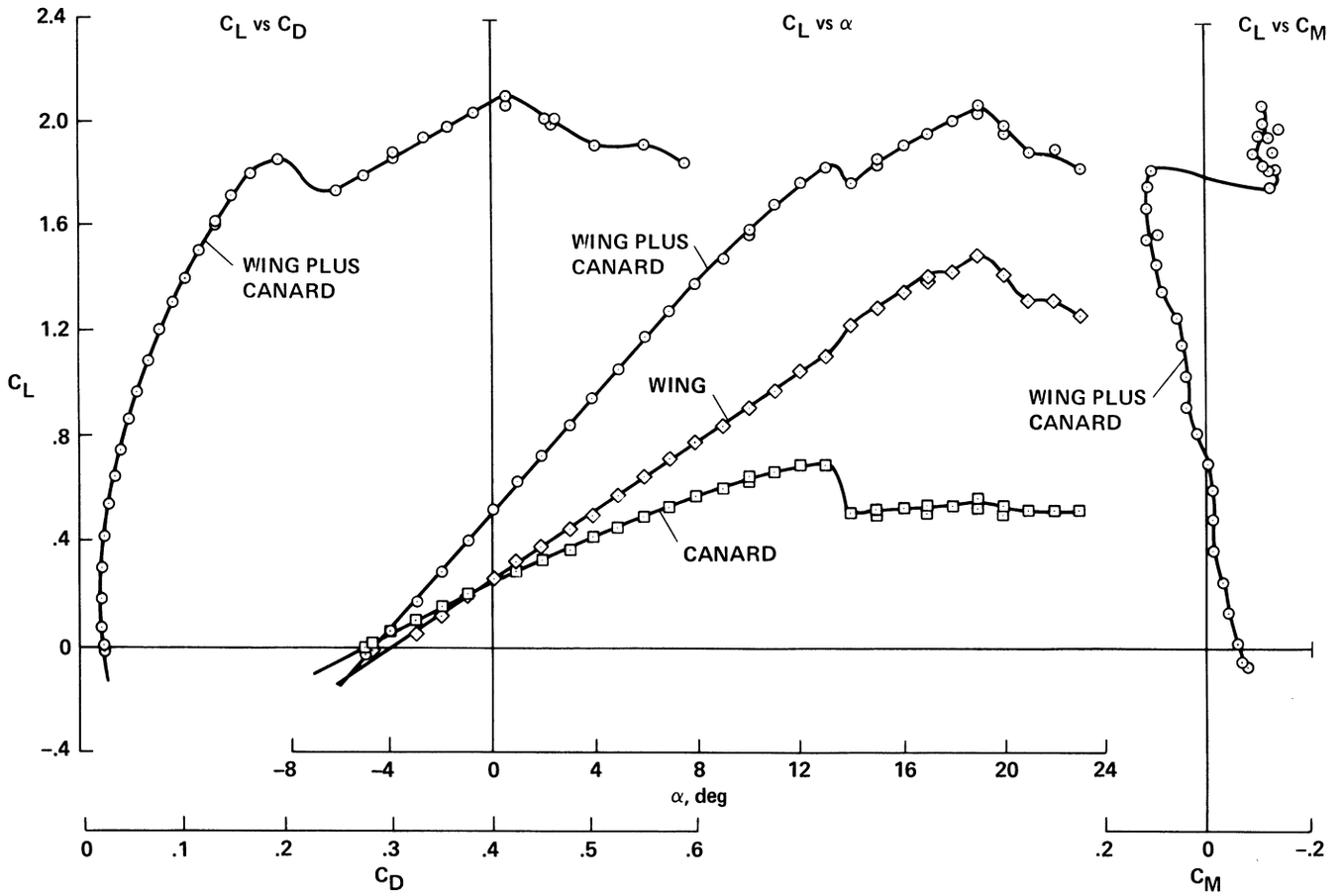

Fig. 3 - Wind-tunnel data for close-coupled wing-canard configurations: canard high ($\bar{\ell}_C = 1.63$, $\bar{g} = +0.5$)

As can be seen, the moment-center location that was used results in a pitching moment curve that is about 10% unstable below stall. To obtain a stable configuration (say 10% stable) the moment-center would have to be moved forward from its present location of 0.54 wing chord forward of the wing quarter chord to a point 0.74 wing chord forward. Also, the pitching moment at zero lift (C_{M_o}) for the configuration tested is negative (nose down), indicating that more canard incidence would be required to trim at a positive C_L for a stable pitching moment configuration. For example, to change C_{M_o} from the present value of $C_{M_o} = -0.07$ to a value $C_{M_o} = +0.07$ would require an increase in canard C_L of $\Delta C_L \cong 0.09$. This could be accomplished by an increase in canard incidence of $\Delta i_c \cong 2°$ to 4°. To obtain a configuration that is (1) stable in pitching moment, (2) trimmed at a C_L in the range 0.5 to 1.0, and (3) such that the canard stalls at an angle of attack close to but less than that of the wing requires that the canard $C_{L_{max}}$ be increased by nearly 100% over the $C_{L_{max}}$ available with the simple GA(W)-2 airfoil section that was tested. This would require a high-lift flap system for the canard.

The effect of the interaction between the wing and the canard can be seen in Fig. 4 where the lift data for the same wing and the same canard, each tested in isolation, are compared with the data shown in Fig. 3. The decrease in wing lift due to the canard downwash and the increase in canard lift due to the wing upwash are evident. An interesting point is the favorable effect of the presence of the canard in extending the wing lift curve to a higher angle of attack before stall and the effect of the presence of the wing in increasing the poststall level of lift of the canard. In addition, the effect of the wing on the canard is to increase the $C_{L_{max}}$ of the canard. All

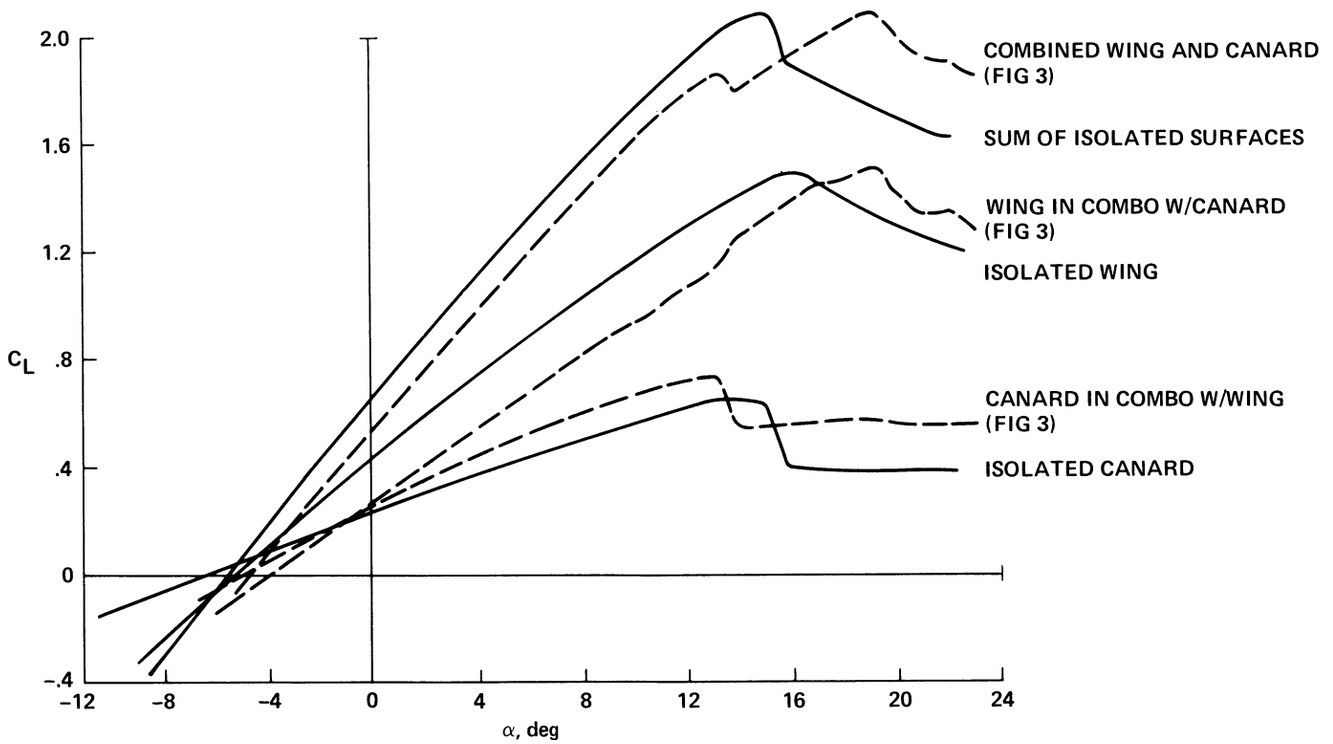

Fig. 4 - Data for isolated surfaces, combined and compared with corresponding data from Fig. 3

of the above effects are seen to result in a $C_{L_{max}}$ for the wing-canard combination for this case that is about as large as the sum of the $C_{L_{max}}$ terms of the isolated surfaces. It appears, however, that if the $C_{L_{max}}$ of the canard were increased, as discussed above, so that the lift-curve peaks of the wing and canard occur at nearly the same angle of attack, then the $C_{L_{max}}$ of the combined wing and canard would exceed that of the sum of the $C_{L_{max}}$ terms of the isolated surfaces. The canard should be designed with appropriate consideration of the actual wing-induced flow field. The effects to be considered are an induced angle of attack increment, increased local velocity, and induced camber. A discussion of the induced camber effect can be found in (6).

EFFECT OF GAP AND STAGGER - The effect of the vertical location of the canard with respect to the wing (gap) is shown in Fig. 5 for the short-coupled case ($\bar{\ell} = 1.63$). Here the wing is mounted 0.5 chord above the level of the canard ("canard low"). The corresponding "canard high" lift data from Fig. 3 are shown superimposed for comparison. The deleterious effect of the low canard location on the wing lift is evident; it is probably caused by the unfavorable interference effect of the tip vortices from the canard passing below the wing instead of over it, as in the canard high-case. Figure 6 shows the data for colinear wing and canard (gap = 0, short-coupled). The lift interference effect here is nearly as favorable as that for the canard-high case, indicating that the canard tip vortices are probably passing over the wing, for the angle-of-attack range of interest. Figures 7

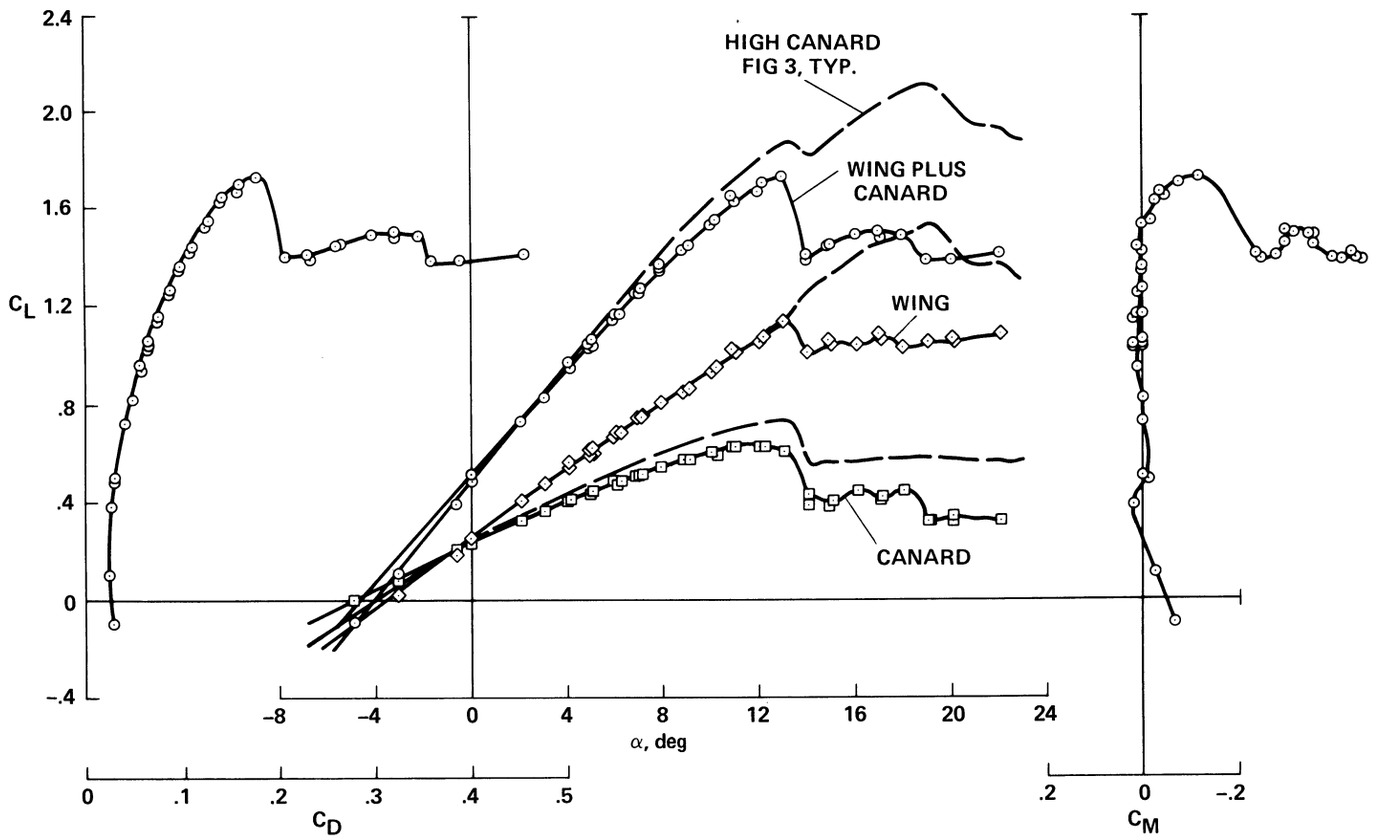

Fig. 5 - Data for close-coupled wing-canard combination: canard low ($\bar{\ell}_C = 1.63$, $\bar{g} = -0.5$)

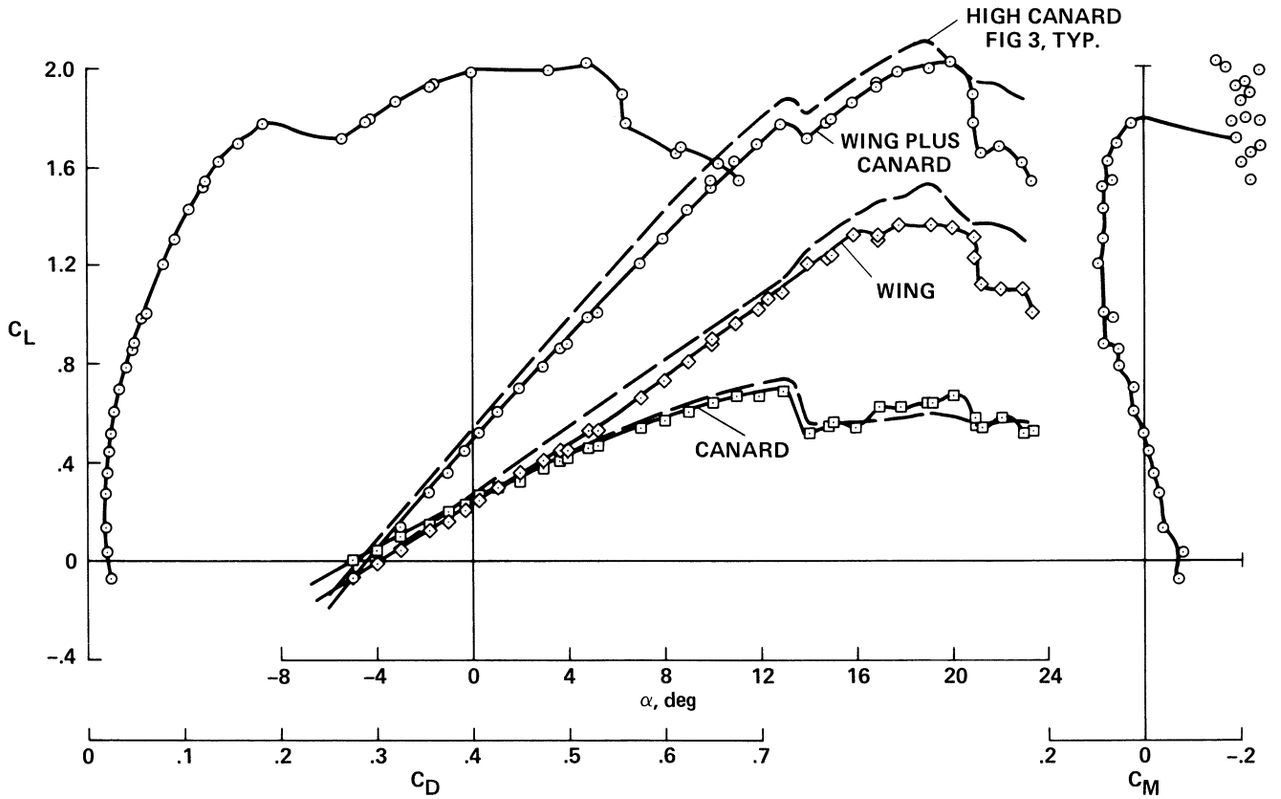

Fig. 6 - Data for close-coupled wing-canard combination: colinear canard ($\bar{\ell}$ = 1.63, $\bar{g}$ = 0)

and 8 show corresponding data for the long-coupled case. Here the horizontal distance between the wing and canard was 3.0 wing chords ($\bar{\ell}$ = 3.0). Figure 7 is for the high-canard case, and Fig. 8 is for the low-canard case; unfortunately, the angle-of-attack range tested for these runs did not always encompass the wing stall angle. The deleterious effect on C_L of the low-canard mounting is not nearly as evident here as it was for the short-coupled cases; apparently, the wing and canard are acting more like two independent surfaces.

These results indicate that a short-coupled, high-canard configuration has some desirable characteristics. The pitching moment stability is linear up to stall and then breaks to a nose-down pitching moment. The $C_{L_{max}}$ of the combined wing-canard configuration was found to equal the sum of the $C_{L_{max}}$'s of the wing and canard in isolation. It appears that the $C_{L_{max}}$ of the combined configuration would exceed that of the sum of the wing and canard in isolation, while still maintaining a favorable stall characteristic, if the $C_{L_{max}}$ of the canard were increased an appropriate amount by use of a high-lift system.

CALCULATED COMPARISONS

The measured results were compared with the results from two theories: a nonlinear vortex-lattice panel method and the classical Prandtl-Munk theory. The vortex-lattice paneling method calculation is shown schematically in Fig. 9. The paneling method is a conventional technique with a bound vortex at the quarter chord of each panel and a control point at the three-quarter chord. The canard and wing camber are included. In addition, the paneling method allows for a free wake

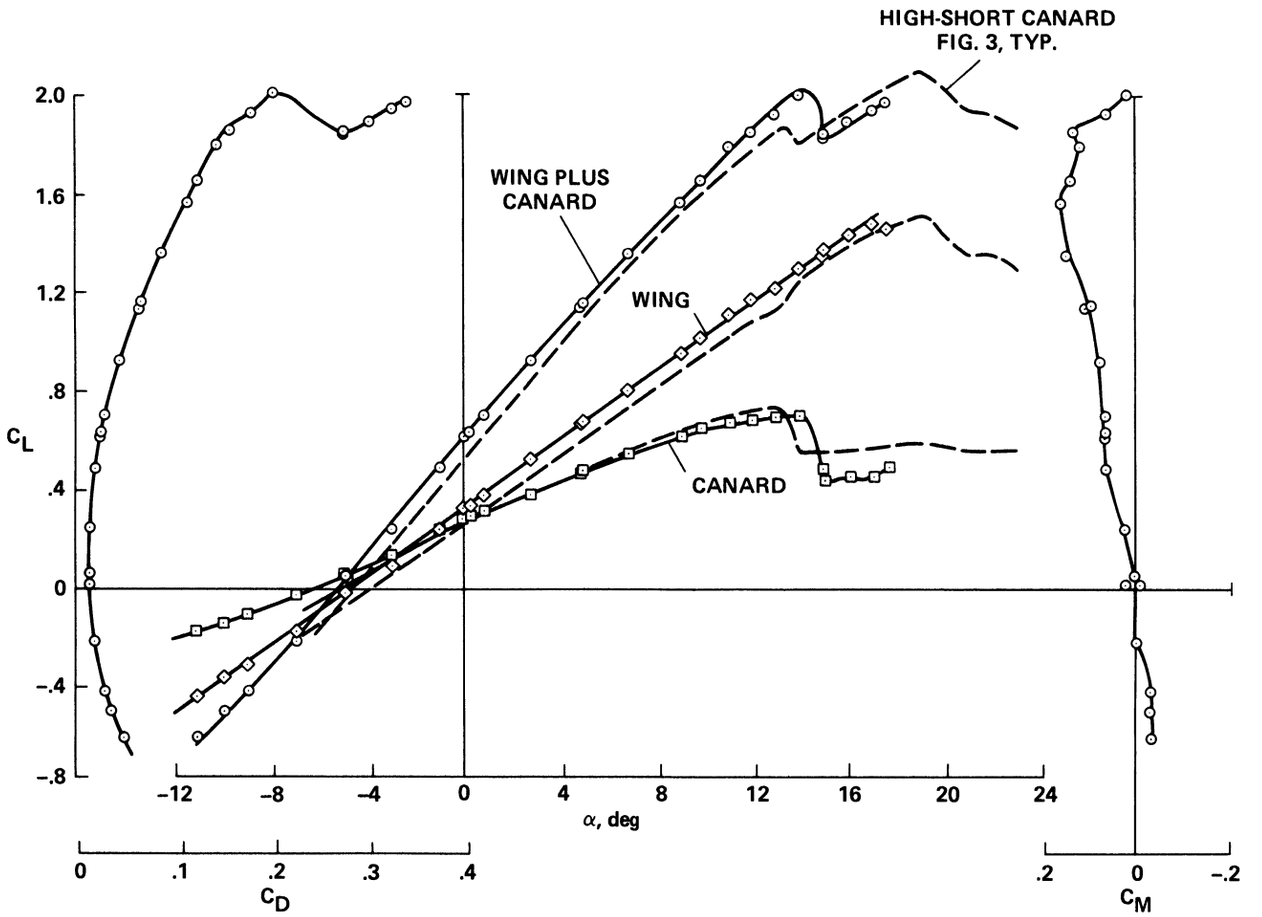

Fig. 7 - Data for long-coupled wing-canard combination: canard high ($\bar{\ell}$ = 3.0, $\bar{g}$ = +0.5)

which is iteratively positioned in a force-free location to provide an accurate assessment of the interference between the canard wake and the wing. Figure 10 shows excellent agreement for the lift vs angle of attack of the wing and canard between the paneling method results and the experimental results shown in Fig. 3. Note that there is a 1.4° discrepancy in the value of the angle of attack for zero lift; it is caused by an inadequate representation of the camber. Also, these data have been corrected for tunnel-wall effects. The Prandtl-Munk theory was used to compute the induced drag according to the following equation:

$$\pi q D_i = \left(\frac{L_w}{b_w}\right)^2 + 2\sigma\left(\frac{L_c}{b_c}\right)\left(\frac{L_w}{b_w}\right) + \left(\frac{L_c}{b_c}\right)^2 \quad (1)$$

The total induced drag consists of a term each for the induced drag of the isolated wing and canard (or tail), based here on elliptic loading for each. The middle term is the induced drag due to interference between the lifting panels. The σ value varies inversely with the gap and is independent of stagger, since the calculation is performed in the Trefftz plane. Figure 11 shows the σ values given in (3). Conventional tunnel-wall corrections were applied to the data for induced drag in order that they could be compared with these theories. Figure 12 shows the magnitude of the wall correction and the magnitude of the tare correction that was discussed previously. The fully corrected data and the results from the panel method and Prandtl-Munk theory are shown in Fig. 13. As can be seen, the experimental

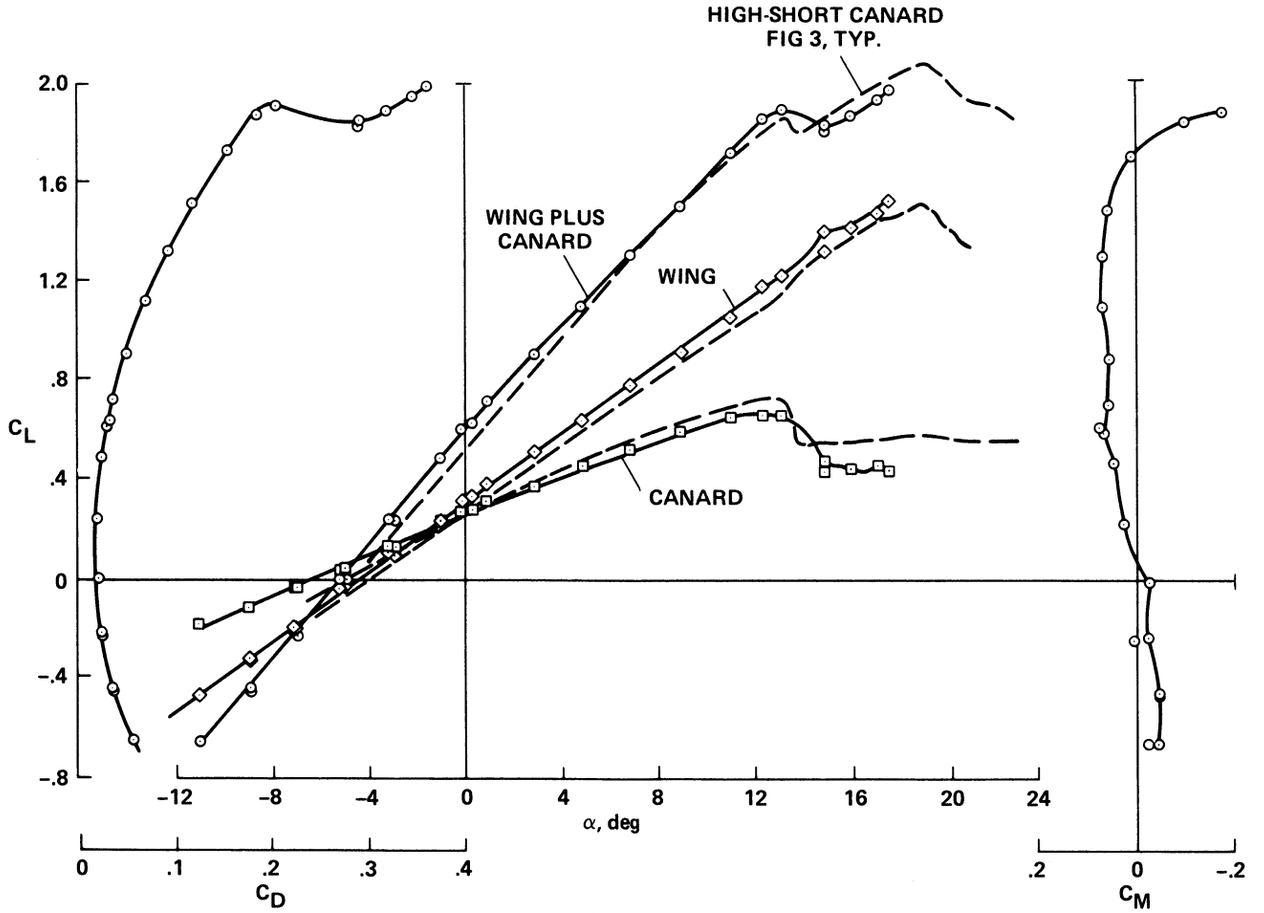

Fig. 8 - Data for long-coupled wing-canard combination: canard low ($\bar{\ell}$ = 3.0, $\bar{g}$ = -0.5)

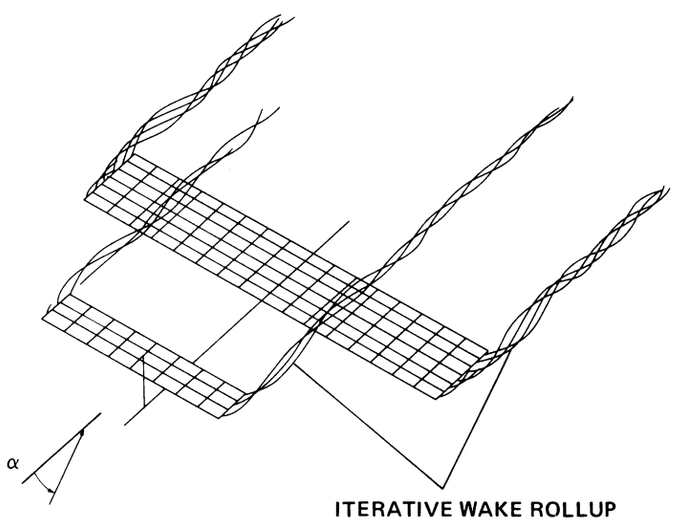

Fig. 9 - Schematic of vortex-lattice paneling method

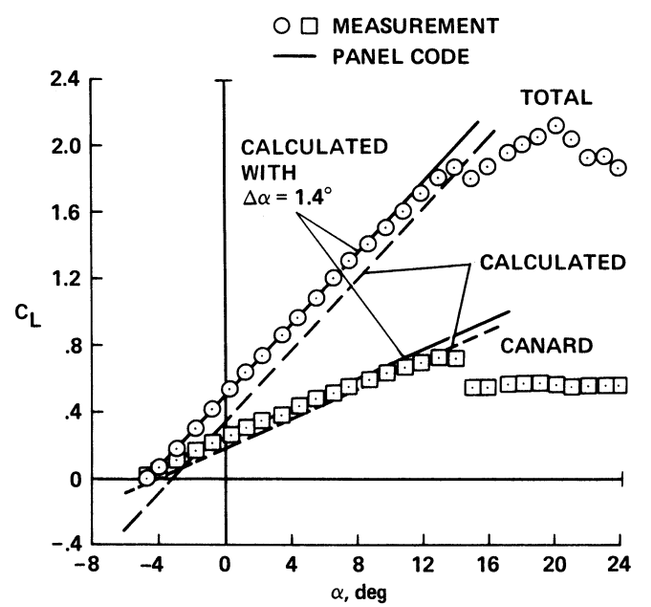

Fig. 10 - Correlation of vortex-lattice paneling method with wind-tunnel data from Fig. 3 ($\bar{\ell}$ = 1.63, $\bar{g}$ = 0.5)

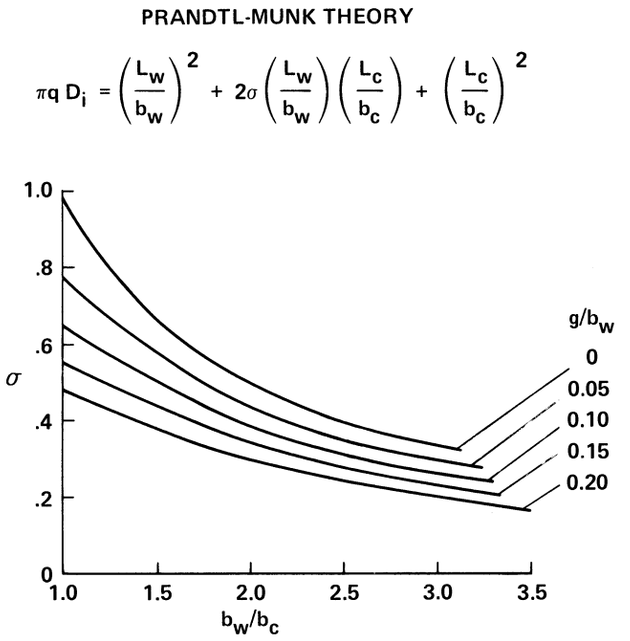

Fig. 11 - Prandtl-Munk interference factor σ for elliptic loading (from (3))

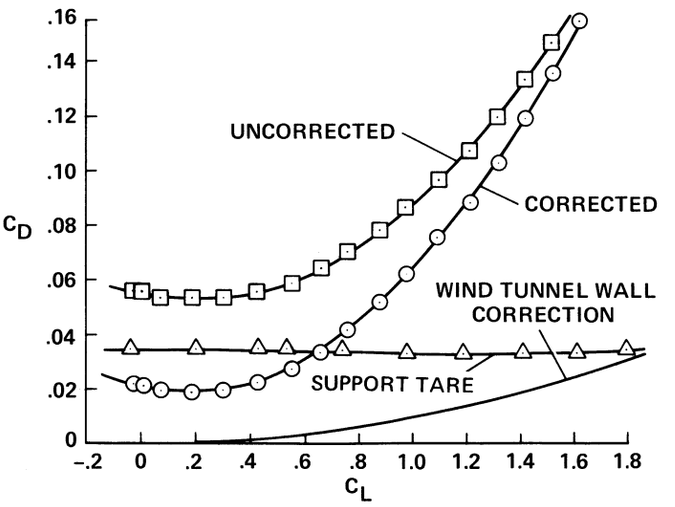

Fig. 12 - Corrections applied to the drag data for comparison with theory ($\bar{\ell}$ = 0.5, $\bar{g}$ = 1.63)

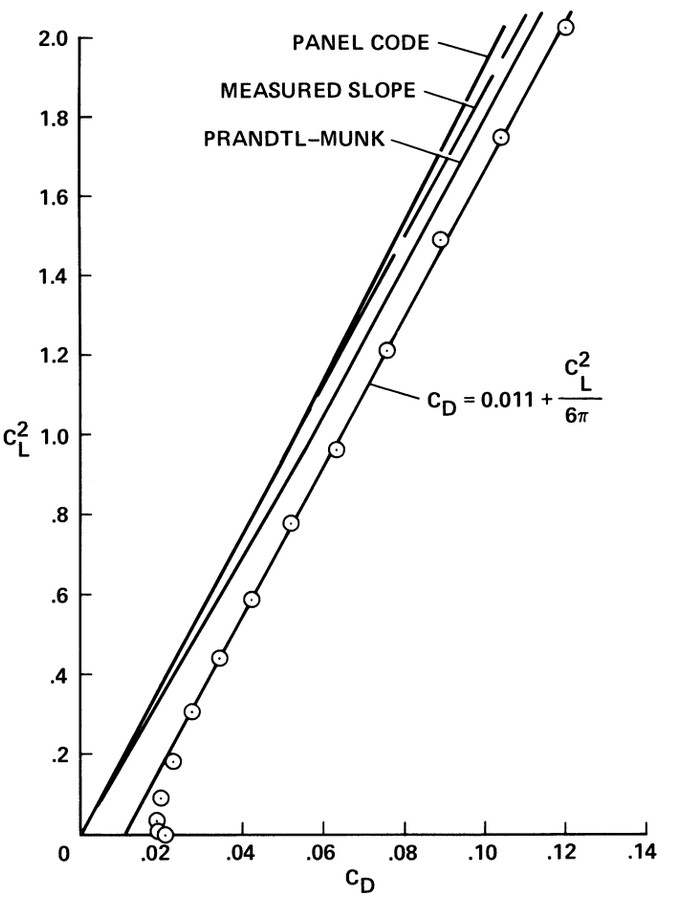

Fig. 13 - Comparison of induced drag determined from the paneling method and Prandtl-Munk theory and the measured results ($\bar{\ell}$ = 0.5, $\bar{g}$ = 1.63)

results are linear over the range $0.3 < C_L^2 < 1.6$ and fit closely to the expression:

$$C_D = 0.011 + C_L^2/6\pi$$

The effective aspect ratio equals 6, which is also the geometric aspect ratio of the wing and canard. The measured slope is shown transferred to the origin for comparison with the theories; agreement with the panel code result is excellent up to $C_L \approx 1.2$, which encompasses the C_L for L/D_{max}. At higher values of C_L, viscous effects are appearing in the experimental data. The Prandtl-Munk result was obtained by using the measured values of wing and canard lift in Eq. (1). The predicted induced drag is seen to be about 10% too high at the C_L for L/D_{max}. Wolkovitch (4) found that this theory was about 14% too high relative to his measurements. In his experiments, however, roughness was applied to the model, whereas in the present experiments it was not. Two-dimensional airfoil data that include both of the airfoil sections used in these experiments are presented in (7) and (8). It appears from these references that a drag bucket occurs in the present tests but not in the

Wolkovitch data. The change in profile drag with lift appears as added induced drag in the present data. The magnitude of this effect is sufficient to account for the differences in the two experiments.

CONFIGURATION COMPARISON - In the following, the Prandtl-Munk theory is used to compare various canard and tail-aft configurations. The lift on each of the two surfaces was obtained by requiring that the configuration be trimmed with a prescribed static margin. A simple expression for lift-curve-slope (found in (9)) was also used. The equations for these considerations and a sketch are presented in Fig. 14; the calculated results appear in Fig. 15. The constant parameters were selected to be representative of commuter-transport configurations; the values appear on the figure. It was found that the L/D of the canard configurations depends strongly on the induced drag of the canard at the C_L for L/D_{max}. The canard C_L (based on the area of the canard) is about double that of the wing for the parameter values used here. These results indicate that the canard aspect ratio is an important parameter. It was found that when the canard aspect ratio equaled that of the

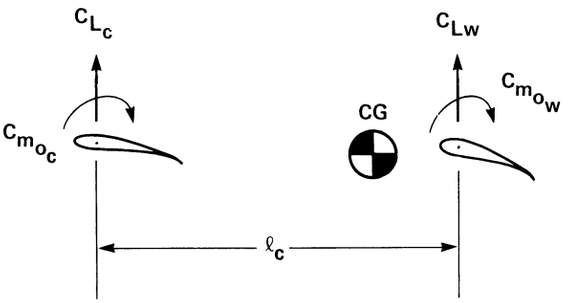

- $\Sigma M_{cg} = 0$
- $\frac{\partial C_m}{\partial C_L}$ = – STATIC MARGIN
- $\frac{\partial C_L}{\partial \alpha} = \frac{2\pi AR}{AR + 3}$

$$C_D = C_{D_0} + \frac{C_{L_w}^2}{\pi AR_w} + \frac{C_{L_c}^2 \bar{S}_c}{\pi AR_c} + \sigma \frac{b_c}{b_w} \frac{2C_{L_c}}{\pi AR_c} C_{L_W}$$

$$C_L = C_{L_w} + C_{L_c} \bar{S}_c$$

Fig. 14 - Equations for trimmed wing-canard analysis

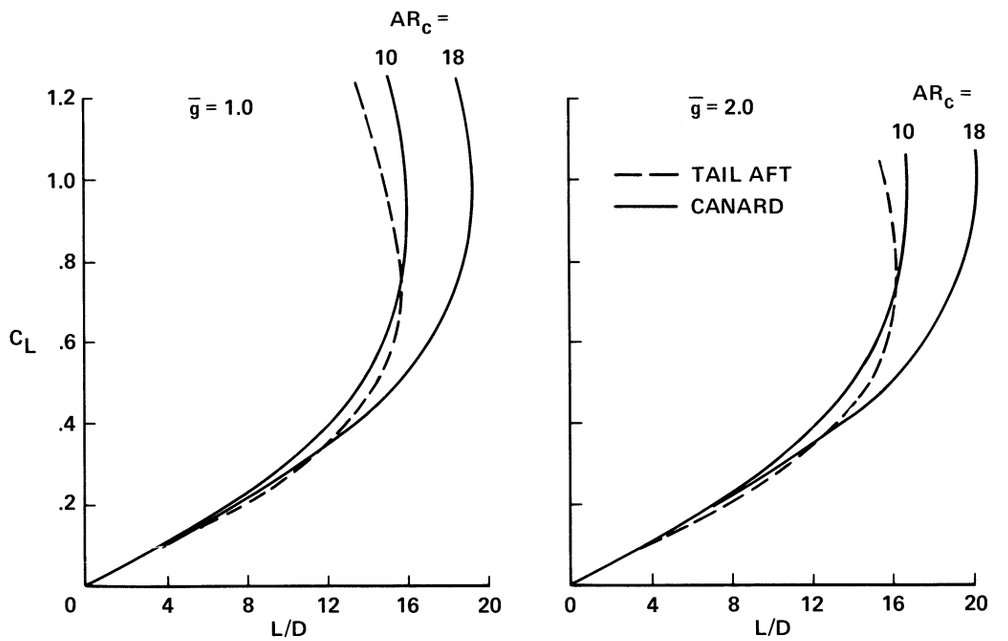

Fig. 15 - Canard vs tail-aft performance, Prandtl-Munk theory, trimmed; static margin = 10%, C_{D_0} = 0.025, AR_w = 10, canard or tail volume = 1.0, AR_t = 6, $\bar{\ell}_t$ = 4, $\bar{\ell}_c$ = 2, $C_{M_{O_W}}$ = -0.2, $C_{M_{O_C}}$ = -0.4

wing, there was essentially no benefit in L/D_{max} over a tail-aft configuration. However, when the canard aspect ratio was 18 and the wing aspect ratio was 10, the maximum L/D was 19-20 (depending on the vertical gap); for the tail-aft configuration, the maximum L/D was about 16.

The significance of the canard-induced drag can also be seen by examining the Prandtl-Munk expression. Equation (1) can be written in the form

$$\frac{C_{D_i}\pi AR_W}{C_L{}^2} = \left(1 - \frac{L_C}{L}\right)^2 \left[1 + \frac{(L_C/L)^2}{(b_C/b_W)^2(1 - L_C/L)^2} + \frac{2\sigma(L_C/L)}{(b_C/b_W)(1 - L_C/L)}\right] \qquad (2)$$

The left-hand side of Eq. (2) is the non-dimensional induced drag based on any reference area. The aspect ratio is based on the largest span of the two panels. In this form, the expression is the reciprocal of the usual span efficiency factor. It depends on the lift ratio (L_C/L), span ratio (b_C/b_W), and the gap (g/b_W) needed to obtain σ from Fig. 11). Figure 16 shows plots of the induced drag values obtained from Eq. (2). When the gap is infinite ($g/b_W = \infty$), the interference term is zero ($\sigma = 0$); this represents the maximum benefit possible from tandem surfaces. For these conditions the induced-drag parameter is seen to be a minimum when the span ratio, $b_C/b_W = 1$, and the lift ratio, $L_C/L = 0.5$. The value of the induced-drag parameter for this condition is 0.5 (i.e., the span efficiency factor equals 2.0). When the gap is reduced, the induced drag increases because of the interference; however, the optimum configuration remains $b_C/b_W = 1$ and $L_C/L = 0.5$. For any value of gap, there is a strong effect of span ratio on induced drag. In addition, for the optimum span ratio there is little change in induced drag over a broad range of lift ratios (L_C/L). For example, for $g/b_W = 0.2$ and $b_C/b_W = 1.0$, the span efficiency factor is greater than 1.28 over the lift ratio range from $L_C/L = 0.3$ to $L_C/L = 0.6$. This lift range corresponds to a wide range of trim conditions.

CONCLUDING REMARKS

Wind-tunnel tests and analyses of the aerodynamics associated with wing-canard combinations in low-speed applications were conducted. The data indicate that the interference between the wing and canard was favorable to the $C_{L_{max}}$ of the canard and that it did not degrade the $C_{L_{max}}$ of the wing, provided the canard was properly located vertically with respect to the wing. Comparison of these measurements with calculated results from a vortex-lattice panel code and from the classical

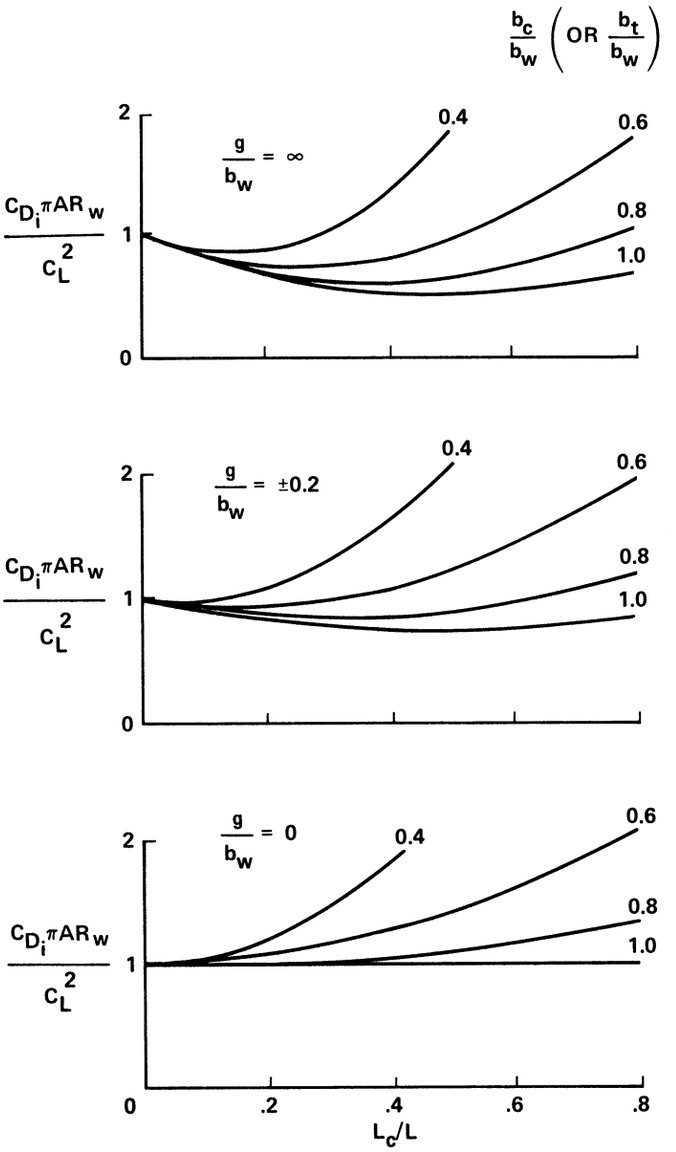

Fig. 16 - Induced drag parameter calculated from Prandtl-Munk theory (Eq. (2))

Prandtl-Munk theory indicated that the panel code gave excellent results for lift and induced drag at moderate C_L. The Prandtl-Munk theory gave conservative results for induced drag. It was found, on the basis of a simple analysis using the Prandtl-Munk theory, that the L/D of a typical commuter transport that was canard-configured could be higher than that for one with tail-aft, if the canard aspect ratio was greater than the wing aspect ratio. An examination of the Prandtl-Munk expression indicated that the ratio of canard span to wing span is important to induced drag and that the optimum configuration, from this consideration, has equal spans. It has been shown here that there are potential advantages — in terms of aerodynamic efficiency, high-lift capability, and stall characteristics — in applying canard and tandem-wing configurations to future aircraft designed to fly in the lower subsonic speed range.

REFERENCES

1. Burt Rutan, "Tale of the Three EZ's." Sport Aviation, Vol. 29, No. 2, Feb. 1980.

2. Milton D. McLaughlin, "Calculations and Comparisons with an Ideal Minimum of Trimmed Drag for Conventional and Canard Configurations Having Various Levels of Static Stability." NASA TN D-8391, May 1977.

3. E. V. Laitone, "Prandtl's Biplane Theory Applied to Canard and Tandem Aircraft." J. Aircraft, Vol. 17, No. 4, Apr. 1980, pp. 233-237.

4. Julian Wolkovitch, "Subsonic V/STOL Aircraft Configurations with Tandem Wings." J. Aircraft, Vol. 16, No. 9, Sept. 1979, pp. 605-611.

5. W. F. Durand, ed, "Aerodynamic Theory." Vol. II, Reprinted by Dover, New York, 1963.

6. Robert B. Addoms and Frank W. Spald, "Aerodynamic Design of High-Performance Biplane Wings." J. Aircraft, Vol. 12, No. 8, Aug. 1975.

7. Robert J. McGhee, William D. Beasley, and Dan M. Somers, "Low-Speed Aerodynamic Characteristics of a 13-Percent Thick Airfoil Section Designed for General Aviation Applications." NASA TM X-72697, May 1977.

8. Robert J. McGhee and William D. Beasley, "Low-Speed Aerodynamic Characteristics of a 17-Percent Thick Airfoil Section Designed for General Aviation Applications." NASA TN D-7428, 1973.

9. Robert T. Jones and Doris Cohen, "High Speed Wing Theory." Princeton Aeronautical Paperbacks, No. 6, Princeton University Press, 1960.